NASA/TM—2019–220166

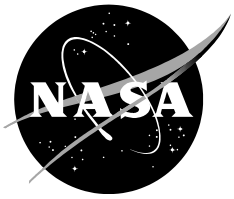

TESS Data Release Notes:
Sector 6, DR8

Michael M. Fausnaugh, Christopher J. Burke
Kavli Institute for Astrophysics and Space Science, Massachusetts Institute of Technology, Cambridge, Massachusetts

Douglas A. Caldwell
SETI Institute, Mountain View, California

Jon M. Jenkins
Ames Research Center, Moffett Field, California

Jeffrey C. Smith, Joseph D. Twicken
SETI Institute, Mountain View, California

Roland Vanderspek
Kavli Institute for Astrophysics and Space Science, Massachusetts Institute of Technology, Cambridge, Massachusetts

John P. Doty
Noqsi Aerospace Ltd, Billerica, Massachusetts

Eric B. Ting
Ames Research Center, Moffett Field, California

Joel S. Villasenor
Kavli Institute for Astrophysics and Space Science, Massachusetts Institute of Technology, Cambridge, Massachusetts

February 27, 2019

Acknowledgements

These Data Release Notes provide information on the processing and export of data from the Transiting Exoplanet Survey Satellite (TESS). The data products included in this data release are full frame images (FFIs), target pixel files, light curve files, collateral pixel files, cotrending basis vectors (CBVs), and Data Validation (DV) reports, time series, and associated xml files.

These data products were generated by the TESS Science Processing Operations Center (SPOC, Jenkins et al., 2016) at NASA Ames Research Center from data collected by the TESS instrument, which is managed by the TESS Payload Operations Center (POC) at Massachusetts Institute of Technology (MIT). The format and content of these data products are documented in the Science Data Product Description Document (SDPDD)[1]. The SPOC science algorithms are based heavily on those of the Kepler Mission science pipeline, and are described in the Kepler Data Processing Handbook (Jenkins, 2017).[2] The Data Validation algorithms are documented in Twicken et al. (2018) and Li et al. (2019). The TESS Instrument Handbook (Vanderspek et al., 2018) contains more information about the TESS instrument design, detector layout, data properties, and mission operations.

The TESS Mission is funded by NASA's Science Mission Directorate.

This report is available in electronic form at
https://archive.stsci.edu/tess/

[1] https://archive.stsci.edu/missions/tess/doc/EXP-TESS-ARC-ICD-TM-0014.pdf
[2] https://archive.stsci.edu/kepler/manuals/KSCI-19081-002-KDPH.pdf

1 Observations

TESS Sector 6 observations include physical orbits 19 and 20 of the spacecraft around the Earth. The first ∼3 days of orbit 19 were used to collect calibration data for measuring the pixel-response function of the cameras under the improved pointing system (introduced in Sector 4). Data collection was paused for 1.09 days during perigee passage while downloading data. In total, there are 20.68 days of science data collected in Sector 6.

Table 1: Sector 6 Observation times

	UTC	TJD[a]	Cadence #
Orbit 19	2018-12-12 17:05:01	1465.21262	171185
Data Collection Start	2018-12-15 18:27:38	1468.26998	173387
Orbit 19 end	2018-12-24 12:27:37	1477.01998	179687
Orbit 20 start	2018-12-25 14:41:37	1478.11304	180468
Orbit 20 end	2019-01-06 13:01:37	1490.04359	189064

[a] TJD = TESS JD = JD - 2,457,000.0

The spacecraft was pointing at RA (J2000): 92.0096°; Dec (J2000): −30.5839°; Roll: 178.6367°. Two-minute cadence data were collected for 20,000 targets, and full frame images were collected every 30 minutes. See the TESS project Sector 6 observation page[3] for the coordinates of the spacecraft pointing and center field-of-view of each camera, as well as the detailed target list. Fields-of-view for each camera with all two-minute targets can be found at the TESS Guest Investigator Office observations status page[4].

1.1 Notes on Individual Targets

Five very bright stars (Tmag $\lesssim$ 2) with large pixel stamps were not processed in the photometric pipeline. Target pixel files with raw data are provided, but no light curves were produced. The affected TIC IDs are 255559489, 238196512, 38877693, 134501440, and 322899250.

Three stars (93279196, 50743458, and 300015238) had very bright stars nearby (93280676, 50743469, and 300015239, respectively). The contaminating flux for these objects is very large, and the pipeline assigns them disjoint photometric apertures that likely causes uncorrected systematic errors in the light curves.

Seven targets (436103278, 269273552, 220393543, 124918771, 124751941, 156934909, and 150110391) had apertures selected (25x25 pixels) that did not fully capture the bleed trails.

1.2 Spacecraft Pointing and Momentum dumps

The reaction wheel speeds were reset with momentum dumps every 3.125 days. FFIs taken during these times are marked with bit 6 (Reaction Wheel Desaturation Events) set. Only

[3] https://tess.mit.edu/observations/sector-6

[4] https://heasarc.gsfc.nasa.gov/docs/tess/status.html

one or two FFIs are affected by each momentum dump. Figure 1 summarizes the pointing performance over the course of the sector based on Fine Pointing telemetry.

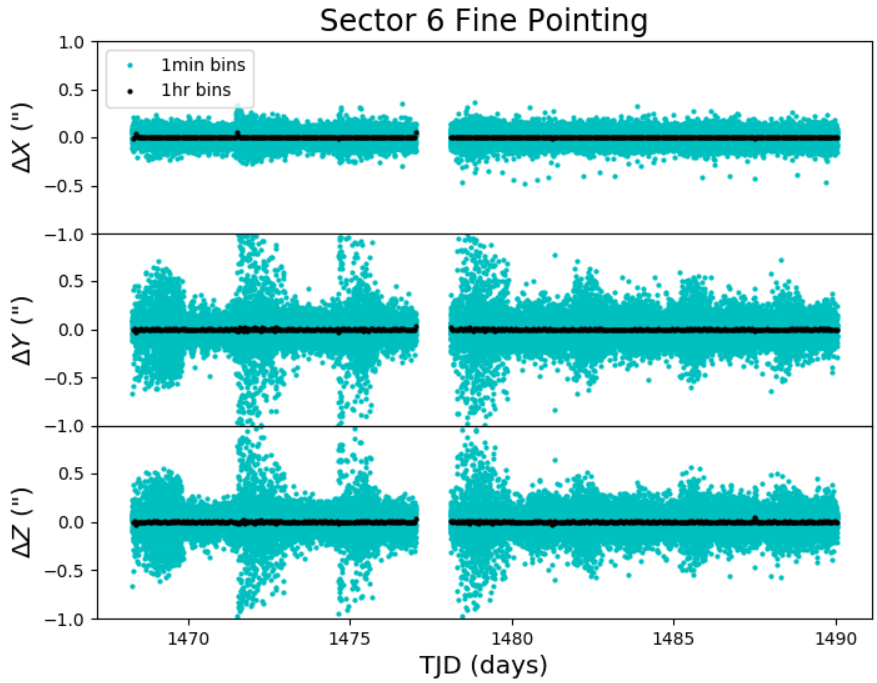

Figure 1: Guiding corrections based on spacecraft fine pointing telemetry. The delta-quaternions from each camera have been converted to spacecraft frame, binned to 1 minute and 1 hour, and averaged across cameras. Long-term trends (such as those caused by differential velocity aberration) have also been removed. The ΔX/ΔY directions represent offsets along the the detectors' rows/columns, while the ΔZ direction represents spacecraft roll.

1.3 Scattered Light

Figure 2 shows the median value of the background estimate for all targets on a given CCD as a function of time. Figure 3 shows the angle between each camera's boresight and the Earth or Moon—this figure can be used to identify periods affected by scattered light and the relative contributions of the Earth and Moon to the image backgrounds. In Sector 6, the main stray light features are caused by the Earth rising above the sunshade at the end of orbit 19, which continues through the start of orbit 20.

2 Data Anomaly Flags

See the SDPDD (§9) for a list of data quality flags and the associated binary values used for TESS data, and the Instrument Handbook for a more detailed description of each flag.

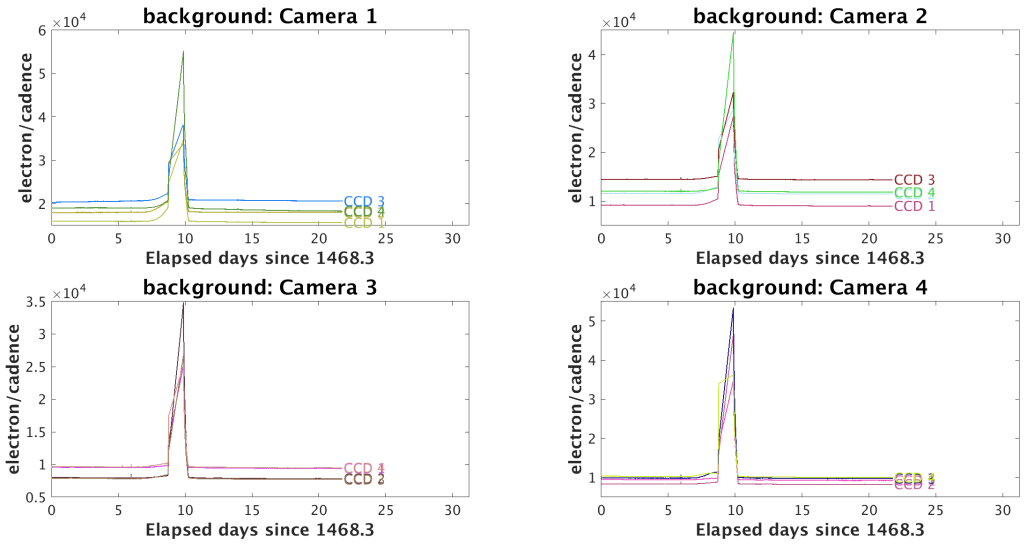

Figure 2: Median background flux across all targets on a given CCD in each camera. The changes are caused by variations in the orientation and distance of the Earth and Moon. The peak between orbits was caused by the Earth rising above the sunshade.

The following flags were not used in Sector 6: bits 1, 2, 7, 9, 11, and 12 (Attitude Tweak, Safe Mode, Cosmic Ray in Aperture, Discontinuity, Cosmic Ray in Collateral Pixel, and Straylight).

Cadences marked with bits 3, 4, and 6 (Coarse Point, Earth Point, and Reaction Wheel Desaturation Event) were marked based on spacecraft telemetry.

Cadences marked with bit 5 and 10 (Argabrightening Events and Impulsive Outlier) were identified by SPOC pipeline results. Bit 5 marks a sudden change in the background measurements. In practice, bit 5 flags are caused by rapidly changing glints and unstable pointing at times near momentum dumps. Bit 10 marks an outlier identified by PDC and omitted from the cotrending procedure.

Cadences marked with bit 8 (Manual Exclude) are ignored by PDC, TPS, and DV for cotrending and transit searches. In Sector 6, these cadences were identified using spacecraft telemetry from the fine pointing system. All cadences with pointing excursions >21 arcseconds (∼1 pixel) were flagged for manual exclude. See Figure 4 for an assessment of the performance of the detrending based on the final set of manual excludes.

FFIs were only marked with bit 6 (Reaction Wheel Desaturation Events). Only one or two FFIs are affected by each momentum dump.

3 Anomalous Effects

3.1 Smear Correction Issues

The following columns were impacted by bright stars in the science frame and/or the upper buffer rows, which bleeds into the upper serial register resulting in an overestimated smear correction.

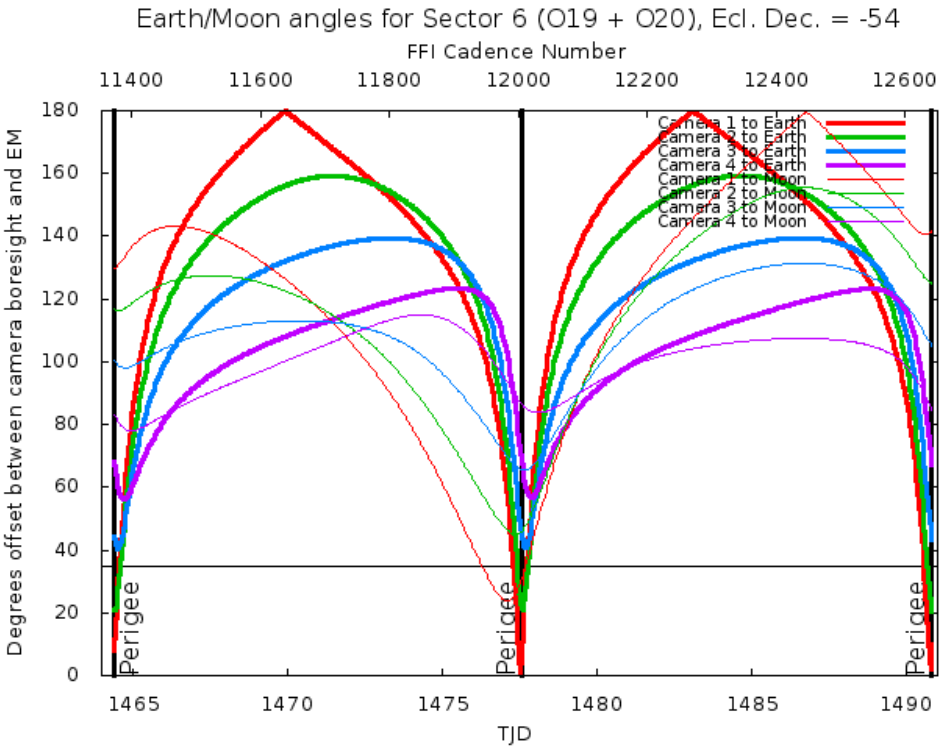

Figure 3: Angle between the four camera boresights and the Earth/Moon as a function of time. When the Earth/Moon moves within 37° of a camera's boresight, scattered light patterns and complicated features such as glints may appear. At larger angles, low level patchy features may appear. This figure can be used to identify periods affected by scattered light and the relative contributions of the Earth and Moon to the background. However, the background intensity and locations of scattered light features depend on additional factors, such as the Earth/Moon azimuth and distance from the spacecraft.

- Camera 1, CCD 4, Columns 652–675, Star Betelgeuse
- Camera 2, CCD 3, Columns 668–692, Star Sirius A
- Camera 2, CCD 4, Columns 1482–1490, Star Arneb
- Camera 4, CCD 4, Columns 507–509, Star AY Dor

3.2 Black Flutter and Popcorn Noise

Flutter in the mean black level was observed in three cameras during Sector 6: camera 2, CCD 2, all outputs, cadences 173550 to 173870 and cadences 181750 to 183250; camera 3, CCD 2, outputs B, C and D, cadences 183000 to 183900; and camera 4, CCD 2, output D, cadences 176340 to 177120.

Popcorn noise in the mean black level was observed in three cameras during Sector 6: camera 1, CCD 3, output C, throughout the first orbit and output A, cadences 176450 to 179687 and cadences 185700 to 186150; camera 3, CCD 1, output B, intermittently

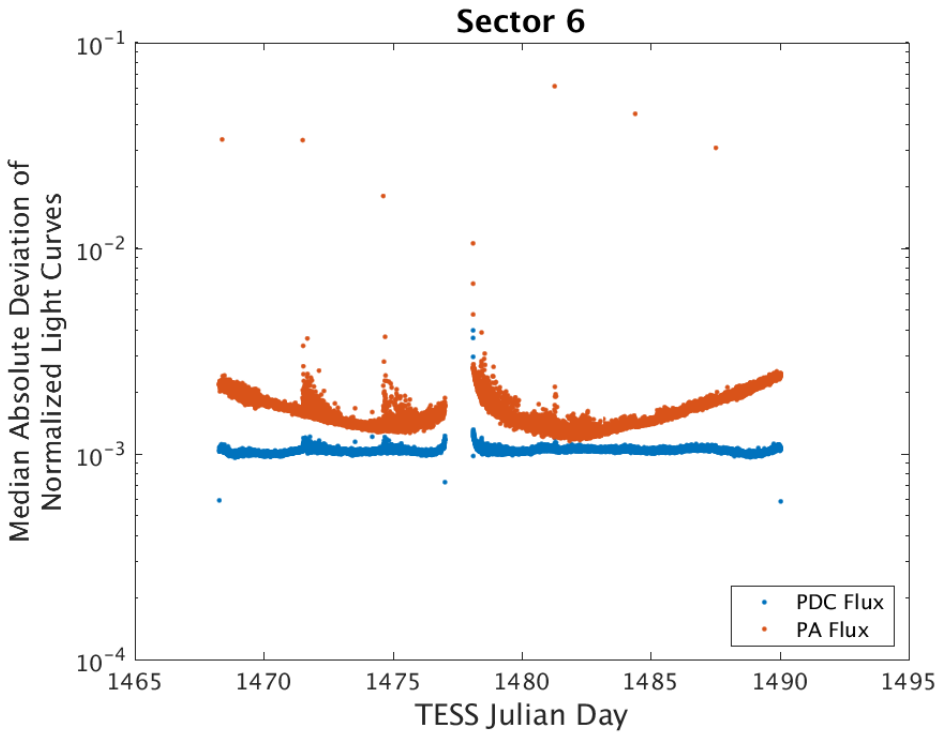

Figure 4: Median absolute deviation (MAD) for the 2-minute cadence data from Sector 6, showing the performance of the cotrending after identifying Manual Exclude data quality flags. The MAD is calculated in each cadence across stars with flux variations less than 1% for both the PA (red) and PDC (blue) light curves, where each light curve is normalized by its median flux value. The scatter in the PA light curves is much higher than that for the PDC light curves, and the outliers in the PA light curves are largely absent from the PDC light curves due to the use of the anomaly flags. Note that the first and last cadences in each orbit are treated as gaps by PDC.

through both orbits; and camera 4, CCD 3, output D, intermittently through both orbits. The time-varying component of the 1-D black model correction removes cadence-to-cadence black variations as well as the black flutter and popcorn noise so the impact to end users is minimal. See the Instrument Handbook §6.3.4 & 6.3.5 for more details about overclock popcorn noise and flutter.

3.3 Fireflies and Fireworks

Table 2 lists all firefly and fireworks events for Sector 6. These phenomena are small, spatially extended, comet-like features in the images that may appear one or two at a time (fireflies) or in large groups (fireworks). See the Instrument Handbook for a complete description.

3.4 TJD Calculation

The spacecraft clock drifts slowly relative to UTC time at a rate of ∼35 milliseconds per day. This drift is captured in a clock kernel that is used to calculate TJD from spacecraft

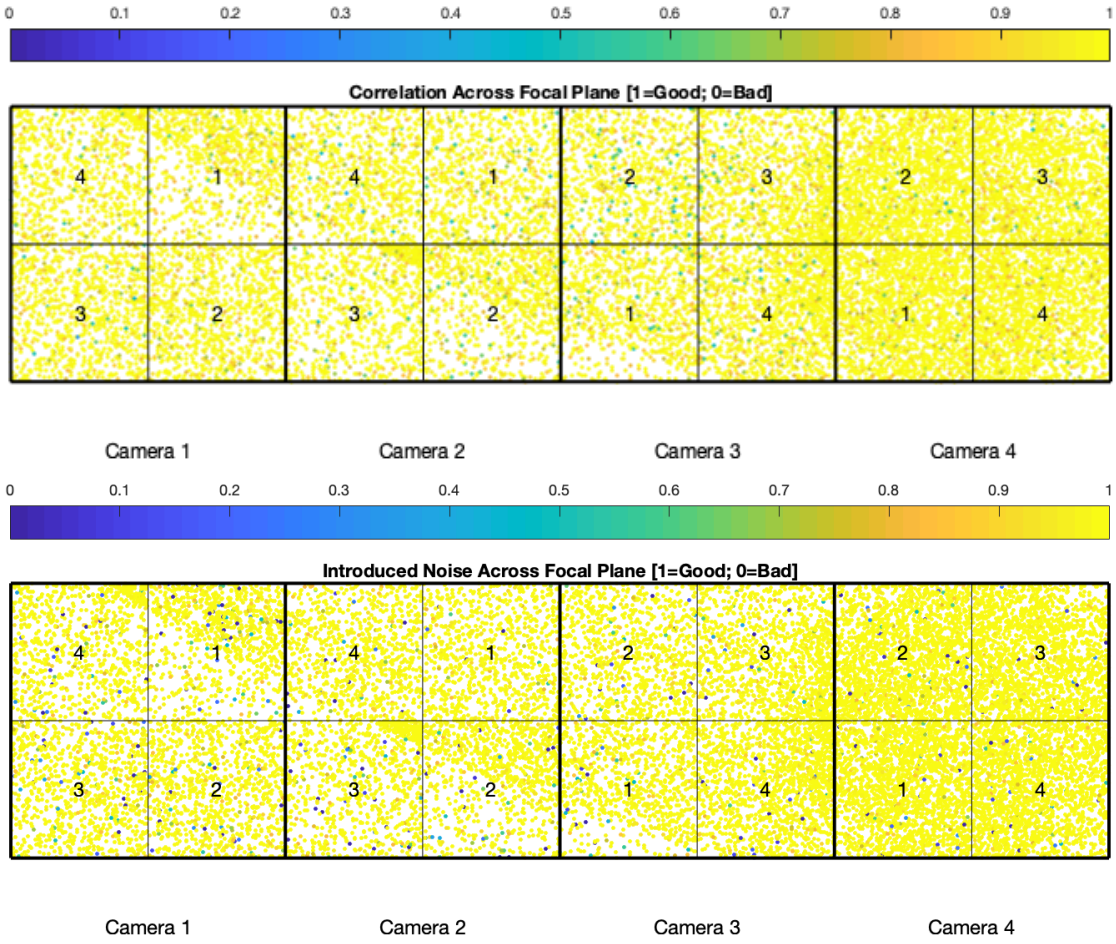

Figure 5: PDC residual correlation goodness metric (top panel) and PDC introduced noise goodness metric (bottom panel). The metric values are shown on a focal plane map indicating the camera and CCD location of each target. The correlation goodness metric is calibrated such that a value of 0.8 means there is less than 10% mean absolute correlation between the target under study and all other targets on the CCD. The introduced noise metric is calibrated such that a value of 0.8 means the power in broad-band introduced noise is only slightly above the level of uncertainties in the flux values.

time. The calculated clock kernel correcting this difference is based on the measured drift rate from periodic S-band and Ka-band ranging contacts.

The clock kernel used to calculate TJD in Sector 6 used ranging data collected only through late August, 2018; as a result, the extrapolation to Sector 6 times is slightly off. The error between true and calculated times grew linearly with time since August 2018, so that the calculated TJD values in all data products are offset from the correct values by $\sim$2.0 seconds at the end of orbit 20 (2019-01-06 UTC). This error also implies that the durations of the individual cadences are underestimated by about 20 microseconds and the FFIs are low by about 280 microseconds, as calculated by the difference between the TSTOP and TSTART times. This issue will be corrected if the data are reprocessed in a future data release.

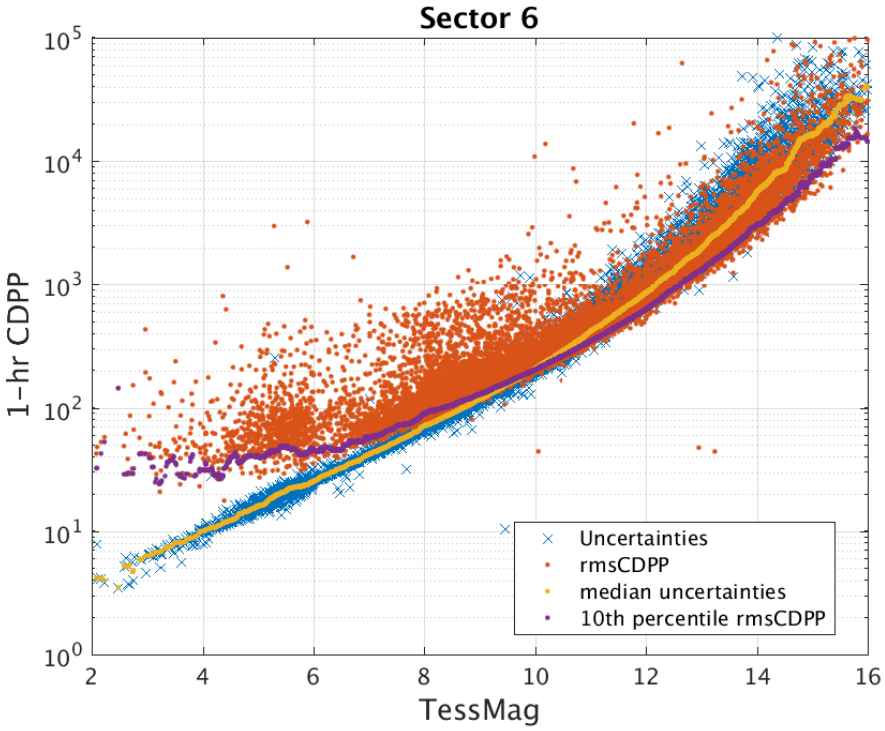

Figure 6: 1-hour CDPP. The red points are the RMS CDPP measurements for the 19,995 light curves from Sector 6 plotted as a function of TESS magnitude. The blue x's are the uncertainties, scaled to 1-hour timescale. The purple curve is a moving 10th percentile of the RMS CDPP measurements, and the gold curve is a moving median of the 1-hr uncertainties.

4 Pipeline Performance and Results

4.1 Light Curves and Photometric Precision

Figure 5 gives the PDC goodness metrics for residual correlation and introduced noise on a scale between 0 (bad) and 1 (good). The performance of PDC is very good and generally uniform over most of the field of view. Figure 6 shows the achieved Combined Differential Photometric Precision (CDPP) at 1-hour timescales for all targets. The performance is a close match to Sector 5, with a systematic error floor between 20–30 ppm (down to Tmag = 10–11).

4.2 Transit Search and Data Validation

In Sector 6, the light curves of 19,995 targets were subjected to the transit search in TPS. Of these, Threshold Crossing Events (TCEs) at the 7.1σ level were generated for 812 targets.

The top panel of Figure 7 shows the distribution of orbital periods for the TPS TCEs found in Sector 6. There is a small excess of TCEs with periods between ~7 and 15 days, with a tendency to pile up near integer multiples of the 3-day spacing between momentum dumps. The bottom panel of Figure 8 shows the number of TCEs at a given cadence that exhibit a transit signal. The isolated peak at the second momentum dump drives most of

Table 2: Sector Fireflies and Fireworks

FFI Start	FFI End	Cameras	Description
2018350102939	2018350105939	3	Firefly
2018352065939	2018352072939	4	Firefly
2018355002939	2018355005939	3, 4	Fireworks
2018355162939	2018355165939	1, 2, 3, 4	Fireworks
2018360075939	2018360082939	2	Firefly
2018361165939	2018361172939	2, 3	Fireflies
2018362162939	2018362165939	2	Firefly
2018363155939	2018363172939	1	Fireworks
2019004155938	2019004162938	4	Fireflies
2019005212938	2019005215938	4	Firefly
2019006092938	2019006095938	3, 4	Firefly

these spurious TCEs. The distribution of TCE transits over cadences is otherwise quite uniform.

The vertical histogram in the right panel of Figure 7 shows the distribution of transit depths derived from limb-darkened transiting planet model fits for TCEs. The model transit depths range down to the order of 100 ppm, but the bulk of the transit depths are considerably larger.

A search for additional TCEs in potential multiple planet systems was conducted in DV through calls to TPS. A total of 1112 TCEs were ultimately identified in the SPOC pipeline on 812 unique target stars. Table 3 provides a breakdown of the number of TCEs by target. Note that targets with large numbers of TCEs are likely to include false positives. Due to proximity to the galactic plane, the targets observed in Sector 6 tend to be more crowded than those observed in prior sectors. As a result, there are a larger number of false positive TCEs due to background sources in Sector 6 than were observed in earlier sectors.

Table 3: Sector 6 TCE Numbers

Number of TCEs	Number of Targets	Total TCEs
1	570	570
2	198	396
3	34	102
4	7	28
5	2	10
6	1	6
–	812	1112

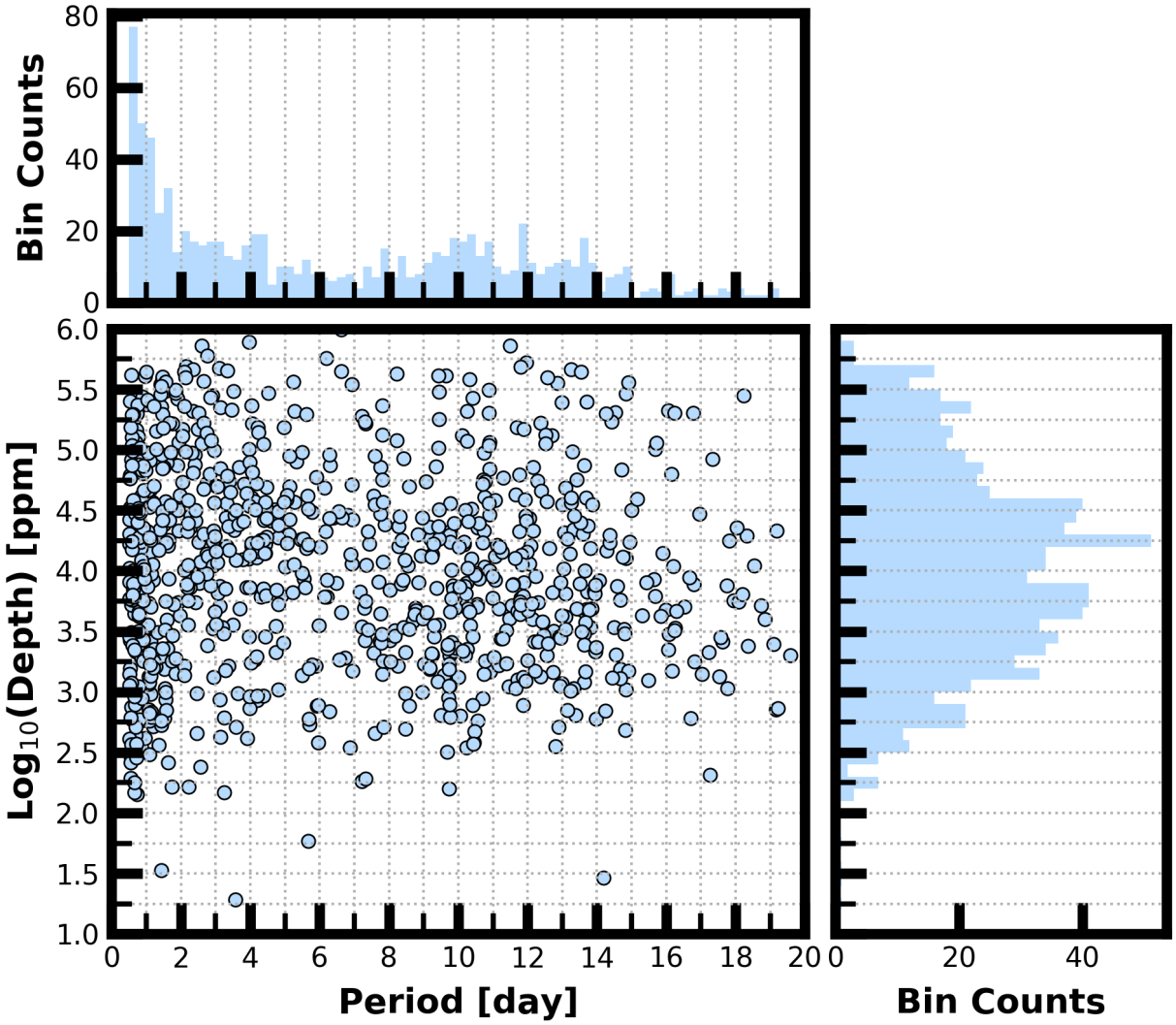

Figure 7: Lower Left Panel: Transit depth as a function of orbital period for the 1112 TCEs identified for the Sector 6 search. For enhanced visibility of long period detections, TCEs with orbital period <0.5 days are not shown. Reported depth comes from the DV limb darkened transit fit depth when available, and when not available, the DV trapezoid model fit depth. Top Panel: Orbital period distribution of the TCEs shown in the lower left panel. Right Panel: Transit depth distribution for the TCEs shown in the lower left panel.

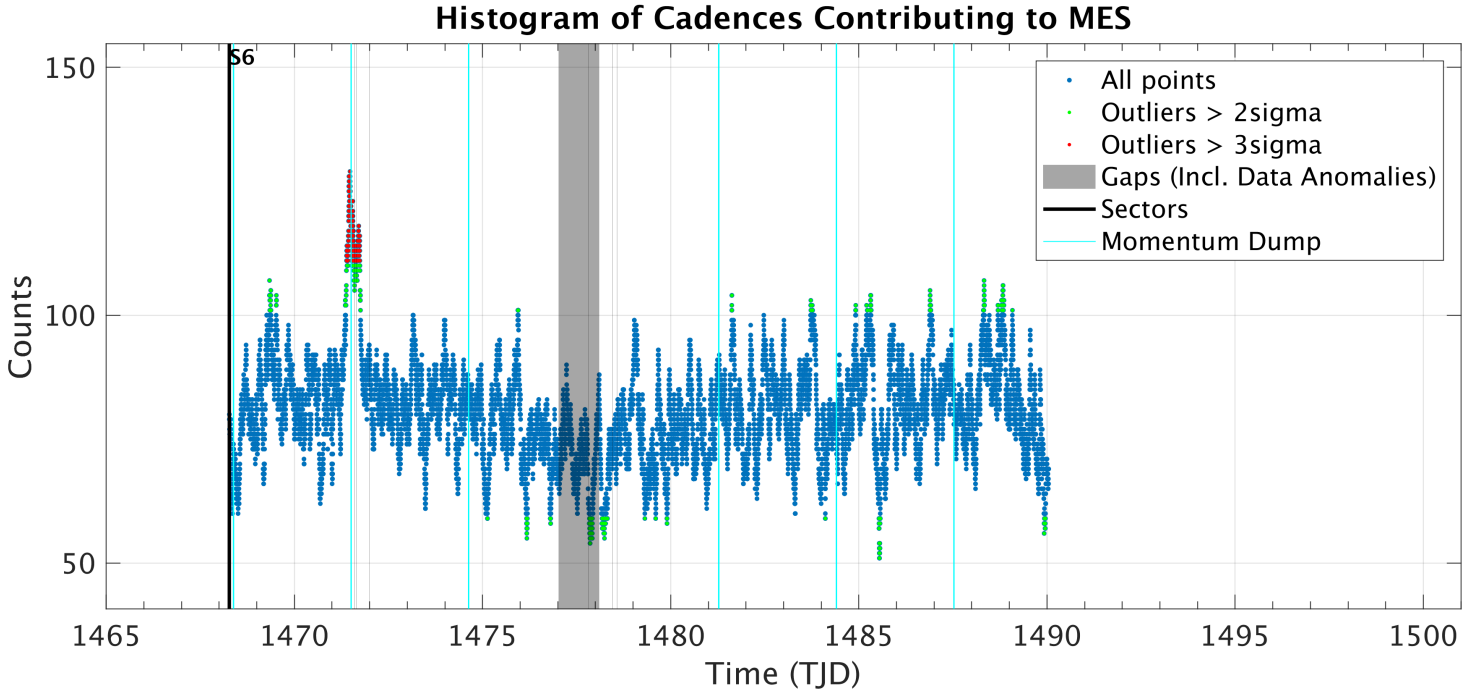

Figure 8: Number of TCEs at a given cadence exhibiting a transit signal. Isolated peaks are caused by a single event and result in spurious TCEs. The peaks typically align with pointing instabilities and strong background variations. The main features to be aware of are cadences impacted by momentum dumps (e.g., TJD epoch 1471.5).

References

Jenkins, J. M. 2017, Kepler Data Processing Handbook: Overview of the Science Operations Center, Tech. rep., NASA Ames Research Center

Jenkins, J. M., Twicken, J. D., McCauliff, S., et al. 2016, in Proc. SPIE, Vol. 9913, Software and Cyberinfrastructure for Astronomy IV, 99133E

Li, J., Tenenbaum, P., Twicken, J. D., et al. 2019, *PASP*, 131, 024506

Twicken, J. D., Catanzarite, J. H., Clarke, B. D., et al. 2018, *PASP*, 130, 064502

Vanderspek, R., Doty, J., Fausnaugh, M., et al. 2018, TESS Instrument Handbook, Tech. rep., Kavli Institute for Astrophysics and Space Science, Massachusetts Institute of Technology

Acronyms and Abbreviation List

BTJD Barycentric-corrected TESS Julian Date

CAL Calibration Pipeline Module

CBV Cotrending Basis Vector

CCD Charge Coupled Device

CDPP Combined Differential Photometric Precision

COA Compute Optimal Aperture Pipeline Module

CSCI Computer Software Configuration Item

CTE Charge Transfer Efficiency

Dec Declination

DR Data Release

DV Data Validation Pipeline Module

DVA Differential Velocity Aberration

FFI Full Frame Image

FIN FFI Index Number

FITS Flexible Image Transport System

FOV Field of View

FPG Focal Plane Geometry model

KDPH Kepler Data Processing Handbook

KIH Kepler Instrument Handbook

KOI Kepler Object of Interest

MAD Median Absolute Deviation

MAP Maximum A Posteriori

MAST Mikulski Archive for Space Telescopes

MES Multiple Event Statistic

NAS NASA Advanced Supercomputing Division

PA Photometric Analysis Pipeline Module

PDC Pre-Search Data Conditioning Pipeline Module

PDC-MAP Pre-Search Data Conditioning Maximum A Posteriori algorithm

PDC-msMAP Pre-Search Data Conditioning Multiscale Maximum A Posteriori algorithm

PDF Portable Document Format

POC Payload Operations Center

POU Propagation of Uncertainties

ppm Parts-per-million

PRF Pixel Response Function

RA Right Ascension

RMS Root Mean Square

SAP Simple Aperture Photometry

SDPDD Science Data Product Description Document

SNR Signal-to-Noise Ratio

SPOC Science Processing Operations Center

SVD Singular Value Decomposition

TCE Threshold Crossing Event

TESS Transiting Exoplanet Survey Satellite

TIC TESS Input Catalog

TIH TESS Instrument Handbook

TJD TESS Julian Date

TOI TESS Object of Interest

TPS Transiting Planet Search Pipeline Module

UTC Coordinated Universal Time

XML Extensible Markup Language